Received February 24, 2020, accepted March 9, 2020, date of publication March 12, 2020, date of current version March 25, 2020.

Digital Object Identifier 10.1109/ACCESS.2020.2980310

A Disease Index for Efficiently Detecting Wheat Fusarium Head Blight Using Sentinel-2 Multispectral Imagery

LINYI LIU[1,2,3], YINGYING DONG[1,3], WENJIANG HUANG[1,3], XIAOPING DU[1,3], BINYUAN REN[4], LINSHENG HUANG[5], QIONG ZHENG[6], AND HUIQIN MA[1,7]

[1]Key Laboratory of Digital Earth Science, Aerospace Information Research Institute, Chinese Academy of Sciences, Beijing 100094, China
[2]College of Resources and Environment, University of Chinese Academy of Sciences, Beijing 100049, China
[3]State Key Laboratory of Remote Sensing Science, Aerospace Information Research Institute, Chinese Academy of Sciences, Beijing 100094, China
[4]National Agricultural Technology Extension and Service Center, Beijing 100125, China
[5]Anhui Engineering Laboratory of Agro-Ecological Big Data, Anhui University, Hefei 230601, China
[6]Key Laboratory of Guangdong for Utilization of Remote Sensing and Geographical Information System, Guangdong Open Laboratory of Geospatial Information Technology and Application, Guangzhou Institute of Geography, Guangzhou 510070, China
[7]Collaborative Innovation Center on Forecast and Evaluation of Meteorological Disasters, School of Applied Meteorology, Nanjing University of Information Science and echnology, Nanjing 210044, China

Corresponding authors: Wenjiang Huang (huangwj@radi.ac.cn) and Yingying Dong (dongyy@radi.ac.cn)

This work was supported in part by the National Key Research and Development Program of China under Grant 2017YFE0122400, in part by the Science and Technology Service Program of Chinese Academy of Sciences under Grant KFJ-STS-ZDTP-054, in part by the National Natural Science Foundation of China under Grant 41601466 and Grant 41601467, and in part by the Youth Innovation Promotion Association CAS under Grant 2017085.

ABSTRACT Rapid, non-destructive detection of wheat *Fusarium* head blight (FHB) is an important tool for disease control. Red-edge (RE) is a prominent spectral feature for determining crop conditions with the potential to enhance the accuracy of monitoring FHB regionally. This study explored the potential of RE for FHB monitoring based on Sentinel-2 Multispectral Instrument (MSI) data. The novel red-edge head blight index (REHBI) was developed to detect FHB at a regional scale. Hyperspectral data at the canopy scale was integrated to simulate Sentinel-2 multispectral reflectance using the relative spectral response (RSR) function of the sensor. Then, many differential and ratio combinations of Sentinel-2 bands that were sensitive to FHB severity were selected. REHBI was established based on these basic vegetation indexes (VIs), and the model developed from REHBI performed best in monitoring FHB severity ($R^2 = 0.82$, RMSE = 10.1). Additionally, the infected canopies with disease index (DI) values between 10 and 50 were classified as slightly diseased canopies. Ordinary least square (OLS) was used to test the performance of REHBI and two conventional VIs, i.e., OSAVI and RDVI, in monitoring slightly diseased canopies; REHBI outperformed these alternatives ($R^2 = 0.69$, RMSE = 3.6). To approximate real agricultural conditions, Poisson noise was added to the simulated Sentinel-2 multispectral data and generalized performance of VIs was evaluated again; REHBI still had the highest R^2 and lowest RMSE values (0.74 and 12.6, respectively). Finally, to validate REHBI's ability to detect FHB infection in agricultural production, it was applied to monitoring FHB in the wheat planting areas of Changfeng and Dingyuan counties from Sentinel-2 imagery. Generally, REHBI performed better in disease monitoring than OSAVI and RDVI. The overall accuracy was up to 78.6%, and the kappa coefficient was 0.51. Experimental results demonstrate that REHBI can be used to monitor FHB.

INDEX TERMS Red-edge, wheat fusarium head blight, Sentinel-2, spectral analysis, disease index.

I. INTRODUCTION

Above half population in the world feed on wheat (*Triticum aestivum* L.), which has extraordinary significance in ensuring national food security [1]. Scab, or *Fusarium* head blight (FHB), is a fungal disease resulted from *Fusarium graminearum (Gibberella zeae)*. It is a major reason for the loss of yield in winter wheat [2]. FHB is important not only because it reduces yield, but also because it reduces the quality and feed value of affected wheat. In addition, *Fusarium graminearum* can produce mycotoxins, including deoxynivalenol (also known as DON or vomitoxin), which can adversely affect livestock and human health when ingested [3]. Traditionally, FHB in wheat is monitored by

The associate editor coordinating the review of this manuscript and approving it for publication was Stefania Bonafoni.

visual inspection of fields, which is time consuming and labor intensive, but also infeasible for thoroughly monitoring disease occurrence and severity over large areas [4]. In practice, only portions of wheat fields are affected by FHB, and the occurrence and spread of these areas are irregular. Therefore, it is a challenge to accurately and effectively monitor FHB distribution.

As an effective method in object detection over large areas, satellite-based remote sensing technology has become a more viable option for monitoring crop diseases [5]. Since changes in morphology, leaf color, chlorosis and transpiration rate of infected plants can be directly extracted from radiometric measurements, crop diseases can be monitored and identified by remote sensing [6]. Besides, satellite-based imagery can be captured on a regular basis, and it is an affordable and independent data source to monitor crop diseases at a large scale[7]. Many satellite-derived multi-spectral image datasets have been used in crop disease monitoring, including MODIS, HJ-CCD, Landsat 8, SPOT-6, and PlanetScope [6]–[10]. However, most previously used data does not contain wavebands covering red-edge (RE) spectral region. RE band is located between the red absorption maximum and high reflectance in the near infrared (NIR) region, and it is a significant spectral characteristic of vegetation, where the transition from chlorophyll absorption to cellular scattering occurs [11]. Previous studies have noted the relevance of RE bands in estimating leaf area index, plant chlorophyll, nitrogen content, and discriminating different crop types based on their different leaf and canopy structures [12]–[15]. These variables are important for determining crop conditions, and thus give RE potential for use in crop disease monitoring.

The swath width of Sentinel-2A satellite is 290 km, and multi-spectral images of 13 spectral bands are provided at various spatial resolutions [16]. Different from the common high-medium resolution satellite data, Sentinel-2A satellite has three RE bands (705 nm, 740 nm, 783 nm) at a 20-m resolution. Since Sentinel-2 can perform several operational reflectance measurements in and near the RE spectral region while increasing the spatial resolution in short revisit time [17], it has a great prospect in crop disease monitoring. By combining Sentinel-2 bands 5 and 6, it is possible to better characterize RE data at a regional scale. As a result, algorithms can be further developed to detect and identify crop diseases using Sentinel-2. For example, Inos *et al.* resampled hyperspectral field spectra of maize using four sensor spectral data sources—Sentinel-2, RapidEye, Quickbird and WorldView-2. By classifying the resampled spectra using random forest algorithm, the three categories of identified disease severity of grey leaf spot can be represented. The kappa value (0.76) and overall accuracy (84%) of Sentinel-2 data analysis were the largest [18]. Liu *et al.* have proposed a spatio-temporal anomaly detection method, which could detect heavy metal-induced stress in rice crops using multi-temporal Sentinel-2 satellite images; their proposed method successfully detected rice under Cd stress, and the coefficients of spatio-temporal variation in rice vegetation indices were stable regardless of whether they were applied to consecutive growth stages or to two different crop years [19].

Vegetation index (VI) is among the most discussed remote sensing techniques and applications. VIs are simple algebraic combination of spectral band values at multiple wavelengths obtained by remote sensing [20]. Owing to the computational simplicity of methods based on VIs, the potential of VIs in disease detection has been investigated by many scholars. For instance, Mahlein *et al.* detected the severity of fungal leaf diseases of sugar using modified chlorophyll absorption integral (mCAI), anthocyanin reflectance index (ARI) and normalized difference vegetation index (NDVI), finding that three sugar beet diseases can be distinctively differentiated using combinations of two or more spectral vegetation indices [21]. Hou *et al.* detected grapevine leafroll disease (GLD) based on the ant colony clustering algorithm (ACCA), and the spectral discrimination and spectral differences between healthy and diseased grapevines were enhanced by an 11-index feature vector. Finally, the classification accuracies of the four infection stages were 94.4%, 75%, 84.6%, and 83.3 %, respectively [22]. By carrying out linear correlation analysis, logistic discriminant analysis, and linear discriminant analysis, Sreekala *et al.* established discriminant models based on VIs to monitor soybean diseases rating; their discriminant models can accurately detect more than 80% healthy plants, but the accuracy of discriminating individual diseases was poor [23]. The above-mentioned studies utilized commonly applied VIs. The nature of host–pathogen interactions can influence physiological and phenological diseases of crops, and the influence on spectral signature is different [24]. Common VIs are not disease specific or disease dependent. Therefore, special indices should be designed for every disease. Zheng *et al.* detected the severity of yellow rust infection based on the red-edge disease stress index (REDSI), and it outperformed other commonly used VIs [16]. Hania *et al.* developed the spectral disease index (SDI) to identify the 'flavescence dorée' grapevine disease, and the classification precision exceeded 90% [24]. Nevertheless, according to our literature review, the design of a disease index for regional FHB monitoring has received limited attention, and no study has considered whether Sentinel-2 MSI images can be used to accurately monitor FHB.

In this study, hyperspectral data from wheat canopies with different severities of FHB were acquired directly in the field. Canopy hyperspectral reflectance was simulated to the reflectance of Sentinel-2 sensor channels using the relative spectral response (RSR) function of the Sentinel-2 MSI sensor. The main objectives of this paper were (i) to select a sensitive differential and ratio combinations of Sentinel-2 bands for identifying different levels of severity of FHB infection in winter wheat; (ii) to develop a new red-edge multispectral disease index to monitor FHB infection; and (iii) map FHB infection using Sentinel-2 satellite imagery at a regional scale.

II. MATERIALS AND METHODS

A. STUDY AREA AND DATA

Two field sites were investigated in this study (Figure 1). The canopy-scale experiments were conducted at Lujiang county (117°13′ 12′′E, 31°29′ 0′′N) and Shucheng county (116°59′34′′E, 31°32′24′′N), in Anhui province, China, where the major crop is winter wheat ('Yangmai 25,' a susceptible wheat cultivar). These regions have a subtropical humid continental monsoon climate with annual precipitation of about 1000 mm, and the average annual temperature is 15°C [25]. The surface elevations of these regions range between 15 and 80 m [26]. The growing season for wheat is from September to June. According to the United States Department of Agriculture (USDA) soil taxonomy, the yellow brown soil in these regions is classified as alfisols [27]. According to the local agricultural management department, FHB is a common disease in these regions.

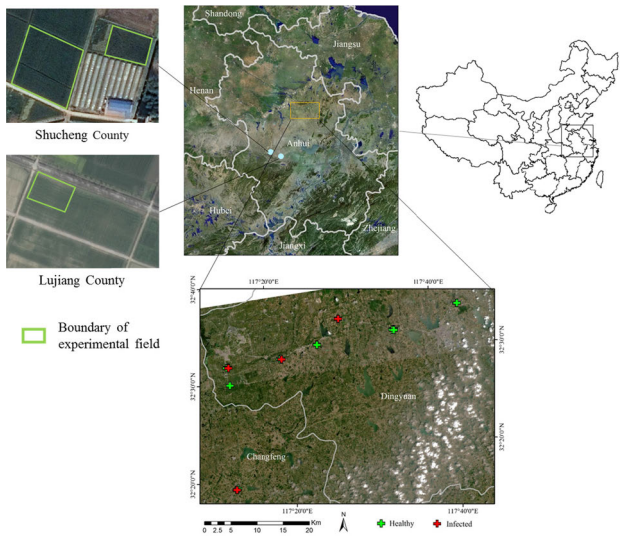

FIGURE 1. The location and sampling sites of the canopy-scale experiments (upper-left) and field surveys of wheat *Fusarium* head blight (FHB) infection (lower-right). The green boxes show the boundaries of experimental fields, while green and red crosses indicate locations that were healthy and infected by FHB, respectively.

Field inspections of wheat FHB infection were carried out in a suburban area of Hefei (117°25′12′′E, 32°30′4′′N), Anhui province. With subtropical humid continental monsoon climate, the annual average temperature of this region is 15.7°C, and the annual average precipitation is 1000 mm. About 50% of the rain occurs from June to August. The terrain tilts from northwest to southeast, and the surface elevation is in the range of 15 ∼ 80 m. With suitable temperature and abundant sunshine, the region is suitable for crop growth. The major crop is winter wheat ('Yangmai 25,' specifically, a cultivar susceptible to FHB) and the major soil type in this region is alfisols. FHB, which is sensitive to local climate and environmental conditions, is reported to be a common disease.

In the canopy-scale experiments, the hyperspectral data of 53 wheat canopies were collected. On May 8, 2018, an ASD FieldSpec Pro spectrometer (Analytical Spectral Devices, Inc., Boulder, CO, USA) was used for the measurement at the grain filling stage of wheat. The spectrometer had the spectral range of 350∼2500 nm, with 3 nm spectral resolution in the 350–1000 nm region and 10 nm spectral resolution in the 1000–2500 nm region [16]. The size of whole field was 42 × 115-m and the crop cultivars, cultivation procedures, and management practices of wheat field were uniform in this place. 53 plots were selected in this field and each plot was around 1 × 1-m. The inner of each plot was homogeneous and there was nearly none bare soil in the plot. According to the field guide for ASD FieldSpec Pro spectrometer, it is important to accurately define the field of view of the sensor and we need to make sure that the size of the plot we wish to measure is large relative to the field of view of the sensor. Considering the measurement of the reflectance spectrum of every plot will be conducted 10 times and the average was taken as the final reflectance spectrum, a circular field of view with radius of 0.1m would be satisfactory. Thus all canopy spectral measurements were taken 1.3 m above the ground in a 25° field of view. The changes in illumination were corrected by performing a 40 × 40-cm $BaSO_4$ calibration panel every 10 measurements. All experiments were carried out between 10:00 and 14:00 under cloudless conditions, and the changes in the solar zenith angle was the minimum. The measurement of the reflectance spectrum of every sample was conducted 10 times, and the average was taken as the final reflectance spectrum. The disease index (DI) of each plot was calculated based on the rules for monitoring and forecasting wheat head blight suggested by the National Plant Protection Department of China (Chinese Standard: GB/T 15796-200X). 10 individual plants were randomly selected in every canopy to detect the disease. All plants were classified into five classes of disease severity according to FHB damage percentage to wheat ears: 0% (class 0), 1–25% (class 1), 26–50% (class 2), 51–75% (class 3), 76–100% (class 4). The DI of each plot was calculated using the formula [28]

$$DI = \frac{\sum (h_i \times i)}{H \times 4} \times 100, \tag{1}$$

where i is the class of disease severity, h_i is the wheat ear number in each class, and H is the quantity of all selected wheat ears. The disease status was evaluated by the continuous variable DI. Moreover, subsequent analysis was carried out by quantitatively classifying the disease severity of the canopy into three classes. Wheat canopies with DI $\leq$ 10 had nearly no symptoms, so canopies with 0 $\leq$ DI $\leq$ 10 were labeled as healthy, canopies with 10 $<$ DI $\leq$ 50 were labeled as slightly diseased, and canopies with 50 $<$ DI $\leq$ 100 were labeled as severely diseased.

In the field inspection at the suburban area of Hefei, 28 plots were investigated in May 2017 (Figure 1). Both our field surveys and interviews with local farmers suggested that the changes in spectral reflectance of these plots are due to the disease of FHB. The sampling was designed according

to the rules for monitoring and forecasting wheat head blight (GB/T 15796-200X). In order to match the spatial resolution of Sentinel-2 multispectral images, the size of each plot is 20 × 20-m.. The inner of each plot was homogeneous and five 1 × 1-m ranges in each plot were investigated to guarantee the uniformity of disease severity in the plot. A submeter-precision handheld global positioning system (GPS) was used to record the central longitude and latitude of every plot. These plots were categorized into two distinct classes: healthy samples and FHB-infected samples.

B. DATA PREPROCESSING

Based on RSR function of the sensor, the hyperspectral data of 53 wheat canopies was integrated for the simulation of the multispectral reflectance of Sentinel-2 using the following equation, so that the potential of Sentinel-2 images for monitoring and detecting wheat FHB monitoring can be evaluated

$$R_{sentinel-2} = \int_{\lambda_{start}}^{\lambda_{end}} f(x)dx, \tag{2}$$

where λ_{start} and λ_{end} are the beginning reflectance wavelength and ending reflectance wavelength of the corresponding Sentinel-2 channel, $R_{sentinel-2}$ denotes the simulated reflectance of the multispectral channel of the Sentinel-2 sensor. $f(x)$ represents RSR function of the Sentinel-2 sensor.

Actual Sentinel-2 multispectral images were obtained from https://scihub.copernicus.eu/. The Sen2cor atmospheric correction toolbox was used to conduct an atmospheric correction for these images in Sentinel Application Platform (SNAP) to remove the effects of the atmosphere on the reflectance values of images [29].

C. USING BASIC VEGETATION INDICES FOR FUSARIUM HEAD BLIGHT DETECTION

When the integration processing of hyperspectral data was finished, two basic vegetation indices, i.e., difference vegetation index (DVI) [30] and ratio vegetation index (RVI) [31], and many modifications of these two indices were calculated. These indices were examined and compared for the detection of FHB using ordinary least squares (OLS). Since we did not have enough samples to partition it into training and test datasets, the leave-one-out cross validation was used to evaluate the generalization performance of models developed from these indices. A correlation analysis was performed between the estimated DI and measured DI. The following equation was used to calculate the root mean square error (RMSE).

$$RMSE = \sqrt{\frac{\sum_{i=1}^{n} \left(y_{est,i} - y_{obs,i}\right)^2}{n}}, \tag{3}$$

where n is the sample size, y_{est} is the estimated DI, and y_{obs} is the observed DI.

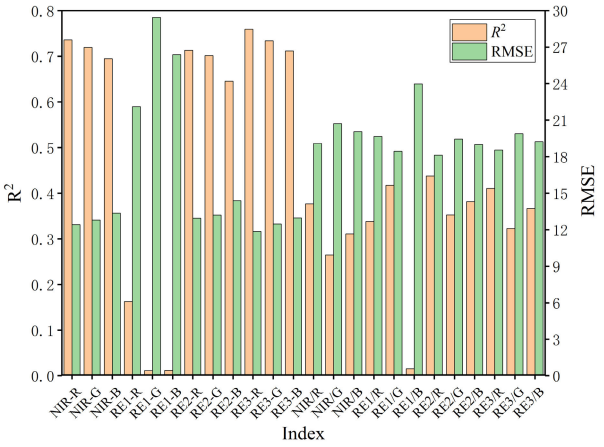

FIGURE 2. The root mean square error (RMSE) and the correlation coefficients (R^2) of models developed using the basic vegetation indices and modified vegetation indices. B, G, R, RE1, RE2, RE3 and NIR are spectral reflectance of blue band, green band, red band, red-edge 1 band, red-edge 2 band, red-edge 3 band and near infrared (NIR) band.

According to the analysis (Figure 2), NIR-R and RE3-R were the most sensitive indices for identifying FHB severity. R, RE3 and NIR are spectral reflectance of red band, red-edge 3 band and near infrared band respectively. In this study, the red-edge head blight index (REHBI) was proposed based on this analysis, and it was the area covered by a triangle in the spectral reflectance space based on the red, red-edge 3, and NIR reflectance values (Figure 3). REHBI was formulated as

$$REHBI = \frac{(842-665)\times(R_{Re3} - R_R) - (783-665)\times(R_{NIR} - R_R)}{2}, \tag{4}$$

where the R_R, R_{Re3}, and R_{NIR} are the red, red-edge 3, and NIR reflectance values. 665, 783 and 842 are central wavelength of the red band, red-edge 3 band, and NIR band, respectively.

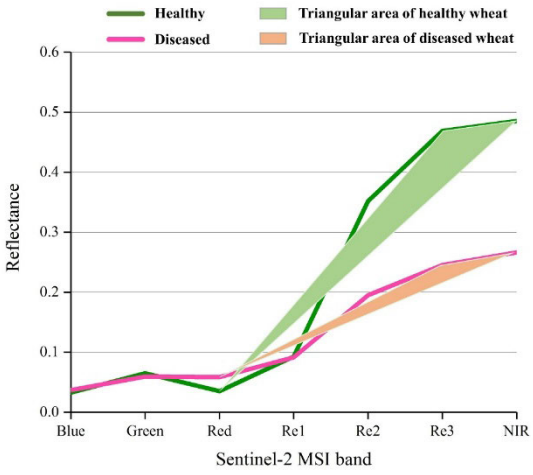

FIGURE 3. A general overview of triangular areas consisting of the red, red-edge 3, and near infrared (NIR) reflectance values for healthy and diseased wheat canopies.

When wheat ears are infected by FHB, the resulting chlorophyll destruction and wheat ear tissue decreases can increase red reflectance and decrease red-edge 3 and NIR reflectance, thus decreasing the total area of the triangle.

D. USING MULTISPECTRAL VEGETATION INDICES FOR FUSARIUM HEAD BLIGHT DETECTION

According to the literature review, crop diseases have been monitored and detected using many VIs [24], [32]–[36]. In this study, apart from REHBI, we also selected fourteen VIs that are widely applied to monitoring disease outbreaks to assess the severity of wheat FHB. These indices were also examined and compared for detecting FHB using OLS, the leave-one-out cross validation was also used to evaluate the generalization performance of models, and the resulted R^2 and RMSE of models developed using these vegetation indices were also calculated. Table 1 contains detailed descriptions of these VIs.

III. RESULTS

A. SPECTRAL CHARACTERISTICS OF DISEASED CANOPIES

Figure 4a indicates that healthy samples, slightly infected samples and severely infected samples are significantly different in the average canopy spectral reflectance. The spectral curve of healthy samples exhibits high reflectance in the NIR region and ''green peak'' and ''red valley'' in the visible (VIS) region, which conforms to the reflectivity of green vegetation. Similar to healthy samples in the red region, samples slightly infected with FHB have spectral reflectance characteristics, and the reflectance are decreased in the green and near infrared regions. Compared with healthy and slightly infected samples, the samples severely infected with FHB have lower reflectance in the near infrared region but higher reflectance in the red region.

The average canopy reflectance of slightly and severely diseased samples and healthy samples in the simulated Sentinel-2 multispectral data is shown in Figure 4b. The reflectance of healthy samples is higher at Re2, Re3, and NIR, while infected samples have decreases at these bands, and the decreases are directly proportional to FHB infection severity. All three kinds of samples have similar reflectance at green and Re1, while severely infected samples have higher reflectance than other samples at red. As shown in Figure 4a, the pattern of the reflectance of the simulated multispectral data in the NIR and visible regions is similar to that of the hyperspectral data.

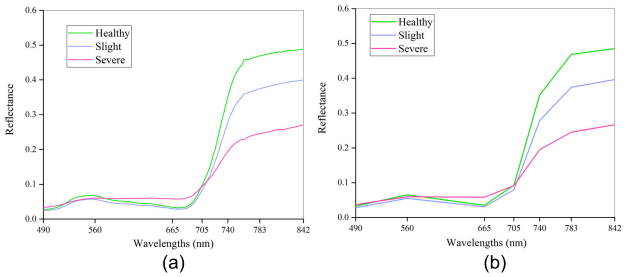

FIGURE 4. Average hyperspectral reflectance (a) and simulated Sentinel-2 multispectral reflectance (b) of healthy (green) and slightly (purple) and severely (red) diseased wheat canopies. Labels in x-axis of chart are central wavelength of the blue band, green band, red band, red-edge 1 band, red-edge 2 band, red-edge 3 band, and NIR band, respectively.

TABLE 1. Characteristics of vegetation indexes (VI_S) used to monitor diseases.

Group	Title	Definition	Description or formula	Reference
Conventional Vis	HBI	Head blight index	$R_G - R_R$	[32]
	NDVI	Normalized Difference Vegetation Index	$(R_{NIR} - R_R)/(R_{NIR} + R_R)$	[37]
	RGR	Ration of red and green	R_R/R_G	[38]
	VARIgreen	Visible atmospherically resistant index	$(R_G - R_R)/(R_G + R_R)$	[39]
	OSAVI	Optimized Soil-Adjusted Vegetation Index	$(R_{NIR} - R_R)/(R_{NIR} + R_R + 0.16)$	[40]
	SR	Simple ratio	R_{NIR}/R_R	[30]
	MSR	Modified simple ratio	$(R_{NIR}/R_R - 1)/((R_{NIR}/R_R)^{0.5} + 1)$	[41]
	GNDVI	Green normalized difference vegetation index	$(R_{NIR} - R_G)/(R_{NIR} + R_G)$	[42]
	RDVI	Re-normalized difference vegetation index	$(R_{NIR} - R_R)/(R_{NIR} + R_R)^{0.5}$	[43]
Red-edge vegetation indices	NDVIre1	Normalized difference vegetation index red-edge1	$(R_{NIR} - R_{Re1})/(R_{NIR} + R_{Re1})$	[37]
	NREDI1	Normalized red-edge1 index	$(R_{Re2} - R_{Re1})/(R_{Re2} + R_{Re1})$	[44]
	NREDI2	Normalized red-edge2 index	$(R_{Re3} - R_{Re1})/(R_{Re3} + R_{Re1})$	[44]
	NREDI3	Normalized red-edge3 index	$(R_{Re3} - R_{Re2})/(R_{Re3} + R_{Re2})$	[44]
	PSRI1	Plant senescence reflectance index	$(R_R - R_G)/ R_{Re1}$	[45]

B. ESTIMATION OF FHB SEVERITY USING SIMULATED MULTISPECTRAL DATA

Table 2 summarizes the R^2 and RMSE values of models developed from REHBI and fourteen commonly used VIs. In general, REHBI performed best among these VIs with R^2 and RMSE values of 0.82 and 10.1, respectively. R^2 values of conventional VIs ranged from 0.29 to 0.77. RDVI performed best among conventional VIs ($R^2 = 0.77$), followed by OSAVI ($R^2 = 0.74$). GNDVI performed worse than other VIs ($R^2 = 0.29$). Among red-edge VIs, R^2 ranged from 0.21 to 0.53. PSRI1 performed best among these VIs ($R^2 = 0.53$), followed by NREDI1 (R^2 of 0.46), while NREDI3 performed worst ($R^2 = 0.21$). As for the average R^2 and average RMSE,

TABLE 2. R^2 and RMSE of models developed from REHBI and fourteen commonly used vegetation indexes (VI_S).

Group	Title	Definition	R^2	RMSE
New index	REHBI	Red-edge head blight index	0.82	10.1
Conventional Vis	HBI	Head blight index	0.60	15.3
	NDVI	Normalized difference vegetation index	0.44	18.1
	RGR	Ratio of red and green	0.49	17.2
	VARIgreen	Visible atmospherically resistant index	0.49	17.2
	OSAVI	Optimized soil-adjusted vegetation index	0.74	12.4
	SR	Simple ratio	0.38	19.1
	MSR	Modified simple ratio	0.41	18.6
	GNDVI	Green normalized difference vegetation index	0.29	20.3
	RDVI	Re-normalized difference vegetation index	0.77	11.5
Red-edge VIs	NDVIre1	Normalized difference vegetation index red-edge1	0.37	19.1
	NREDI1	Normalized red-edge1 index	0.46	17.8
	NREDI2	Normalized red-edge2 index	0.42	18.4
	NREDI3	Normalized red-edge3 index	0.21	21.5
	PSRI1	Plant senescence reflectance index	0.53	16.5

the models developed from conventional VIs performed better than those models developed from red-edge VIs.

When the symptoms are completely exhibited, the observation of FHB is too late for preventative measurement. Therefore, it is important to detect FHB in crops that are only slightly diseased. In this study, canopies were quantitatively classified, and canopies with intermediate DI values (i.e., $10 < DI \leq 50$) were labeled as slightly diseased. OLS was also used to test the performance of REHBI, OSAVI, and RDVI in monitoring slightly diseased canopies. Figure 5 demonstrates that the scatter plots of the estimated DIs and the measured DIs help to visually evaluate the performance of various models using VIs. In general, REHBI performed better than OSAVI and RDVI ($R^2 = 0.69$, RMSE = 3.6 versus $R^2 = 0.34$, RMSE = 5.2 and $R^2 = 0.58$, RMSE = 4.2, respectively), indicating that REHBI was able to accurately identify slightly diseased fields, while OSAVI performed worst among these three VIs.

C. ESTIMATION OF FHB SEVERITY USING NOISY SIMULATED MULTISPECTRAL DATA

In practice, lossy compression of remote sensing images can be influenced by noise of sensors during image capturing [46]. Poisson or signal-dependent (Poisson-like) noise is most frequently observed in remote sensing data and can

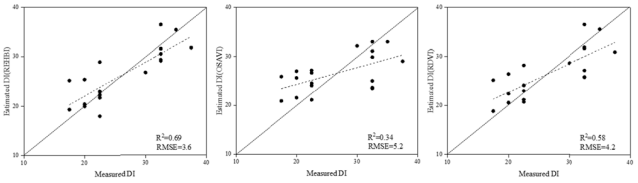

FIGURE 5. Scatter plots of models developed from REHBI, OSAVI, and RDVI for slightly diseased canopies.

TABLE 3. R^2 and RMSE of models developed from REHBI and fourteen commonly used VI_S with and without noise.

Group	Title	With noise		Without noise	
		R^2	RMSE	R^2	RMSE
New index	REHBI	0.74	12.6	0.82	10.1
Conventional VIs	HBI	0.17	22	0.6	15.3
	NDVI	0.26	20.8	0.44	18.1
	RGR	0.09	23.1	0.49	17.2
	VARIgreen	0.06	23.4	0.49	17.2
	OSAVI	0.61	15.1	0.74	12.4
	SR	0.09	23.1	0.38	19.1
	MSR	0.14	22.4	0.41	18.6
	GNDVI	0.25	20.9	0.29	20.3
	RDVI	0.69	13.4	0.77	11.5
Red-edge vegetation indices	NDVIre1	0.22	21.4	0.37	19.1
	NREDI1	0.26	20.8	0.46	17.8
	NREDI2	0.28	20.5	0.42	18.4
	NREDI3	0.1	22.9	0.21	21.5
	PSRI1	0.04	23.6	0.53	16.5

corrupt remote sensing images since it is associated with the particle nature of light [47]. To approach real-world conditions, Poisson noise was added to the hyperspectral data, and the multispectral reflectance of Sentinel-2 data was simulated again. The monitoring models were also developed based on OLS and the leave-one-out cross validation was also used to evaluate the generalization performance. In general, when using noisy data, REHBI still performed best among these VIs ($R^2 = 0.74$, RMSE = 12.6). R^2 values of conventional VIs ranged from 0.06 to 0.69, and RMSE ranged from 13.4 to 23.4. RDVI performed best among conventional VIs ($R^2 = 0.69$), followed by OSAVI ($R^2 = 0.61$). while VARIgreen performed worst ($R^2 = 0.06$). Among red-edge VIs, R^2 ranged from 0.04 to 0.28. NREDI2 performed best among these VIs ($R^2 = 0.28$), followed by NREDI1 ($R^2 = 0.26$), while PSRI1 performed worst ($R^2 = 0.04$). In terms of the average R^2 and RMSE values, the models developed from conventional VIs performed better than those models developed from red-edge VIs. Based on the performance of all VIs before and after adding Poisson noise, all VIs had higher RMSE values and lower R^2 values when using noisy data. This indicates that the difference between DIs predicted by models and the DIs measured became larger after adding Poisson noise.

D. MAPPING DISEASES AT REGIONAL SCALES USING REHBI

The ability of REHBI to detect FHB infection in practice is validated in this study. Potential FHB infection in the

wheat planting areas of Changfeng and Dingyuan counties was monitored by applying REHBI to Sentinel-2 imagery. The temporal dynamics of FHB are primarily influenced by temperature and humidity. Thus, the average land surface temperature (LST) and precipitation from April to May were recorded as environmental features using Climate Hazards Group Infrared Precipitation with Station data (CHIRPS) and MOD11A1. In this study, the support vector machine (SVM) with radial basis function kernel was applied to establish a discrimination model and 28 plots investigated in field inspection at the suburban area of Hefei were used to train and validate the model. The value of regularization parameter and Gaussian width were set as 100 and 1.2 respectively. REHBI, OSAVI, and RDVI were combined with average LST and precipitation from April to May respectively as SVM inputs, and the leave-one-out cross validation was used to extract the confusion matrix to evaluate the generalization performance of models. Specifically, before training the model, a sample was taken from all samples. Then, based on the rest samples, models were trained using three training datasets: a dataset consisting values of REHBI, average LST and average precipitation of rest samples; a dataset consisting values of OSAVI, average LST and average precipitation of rest samples; a dataset consisting values of RDVI, average LST and average precipitation of rest samples. After the models had been trained, the values of REHBI, OSAVI, RDVI, average LST and average precipitation of the sample taken from all samples at first were used to predict the label of this sample through the trained models. These steps were iterated until the labels of all samples have been predicted. The confusion matrix was extracted based on the predicted labels and true labels of all samples. The infection map of FHB produced using REHBI, average LST and average precipitation was showed in Figure 6. The performances of REHBI, OSAVI, and RDVI in FHB monitoring are shown in Table 4. OSAVI and RDVI had the same accuracy indices for disease classification, indicating that OSAVI and RDVI are similarly able to monitor FHB. However, REHBI outperformed OSAVI and RDVI in disease monitoring.

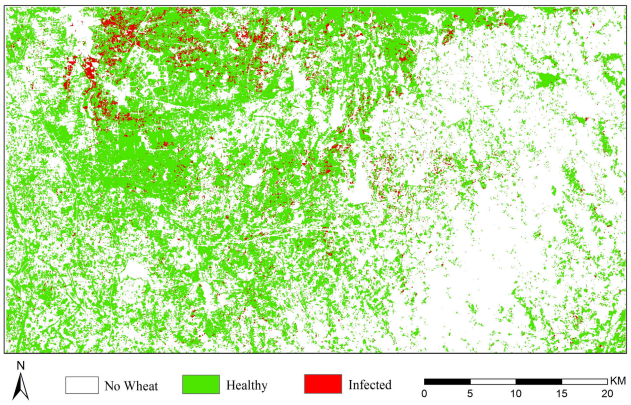

FIGURE 6. **The infection map of *Fusarium* head blight (FHB) in the wheat planting areas of Changfeng and Dingyuan counties produced by the REHBI-based model. Red represents estimated infected wheat, and green represents estimated healthy wheat.**

TABLE 4. **Overall verification results of models developed from REHBI, OSAVI, and RDVI.**

		Reference			User's accuracy (%)	Overall accuracy (%)	Kappa
		Healthy	Diseased	Sum			
REHBI	Healthy	16	3	19	84	78.6	0.51
	Diseased	3	6	9	67		
	Sum	19	9	28			
	Producer's accuracy (%)	84	67				
	TP rate (%)	84	67				
	Type I error	16	33				
	TN rate (%)	67	84				
	Type II error	33	16				
OSAVI	Healthy	17	6	23	74	71.4	0.26
	Diseased	2	3	5	60		
	Sum	19	9	28			
	Producer's accuracy (%)	89	33				
	TP rate (%)	89	33				
	Type I error	11	67				
	TN rate (%)	33	89				
	Type II error	67	11				
RDVI	Healthy	17	6	23	74	71.4	0.26
	Diseased	2	3	5	60		
	Sum	19	9	28			
	Producer's accuracy (%)	89	33				
	TP rate (%)	89	33				
	Type I error	11	67				
	TN rate (%)	33	89				
	Type II error	67	11				

IV. DISCUSSION

Our analyses were able to discriminate among slightly and severely FHB-infected wheat crops and healthy wheat crops based on their significant differences in average canopy spectral reflectance. Figure 4a demonstrates that the samples slightly infected with FHB had similar spectral reflectance properties with healthy samples in red regions, while the spectral reflectance decreased slightly in green region regions. This appears to be caused by or associated with FHB. During favorable weather, salmon-orange to pink spores occur at the base of infected kernels of the fungus [48]. Adjacent kernels are infected by the spores. When DI $\leq$ 50, the damaged area of wheat kernels is always small, with most parts of each wheat kernel still having chlorophyll a, chlorophyll b, and carotenoids. Thus, healthy samples and slightly infected samples have similar average canopy spectral reflectance in the VIS region. When DI $>$ 50, most parts of wheat kernels are infected, and these infected kernels are wrinkled, shrunken, and light [49]. Chlorophyll content degradation and pronounced water loss lead to pronounced variation in spectral properties of infected grains and whole ears, causing the observed significant difference in average canopy spectral reflectance between severely infected samples and healthy samples in NIR and VIS regions. As shown in Figure 4b, it is obvious that simulated multispectral data and hyperspectral data exhibit similar patterns.

Healthy samples and severely infected samples at Red, Re2, Re3, and NIR are significantly different in spectral reflectance, while the spectral reflectance of each sample type is similar at Re1. The central wavelength of Re1 is 705 nm and the band width is 15 nm, i.e., the boundary of the region where reflectance is dominated by pigments and at the beginning portion of the rising slope in NIR caused by structural characteristics [11]. Therefore, a transition from the dominant effect of pigment absorption on NIR vegetative characteristics (i.e., scattering) occurs in this region. This may explain the similar reflectance of healthy samples and severely infected samples in Re1.

Table 2 shows the R^2 and RMSE values of models developed from REHBI and fourteen commonly used VIs. The model developed from RDVI performed best among conventional VIs, followed by OSAVI; a model developed from NDVI yielded lower accuracy. RDVI and OSAVI were both established to improve the sensitivity of NDVI to soil backgrounds [20]. The good performances of these indices indicated that even if FHB occurred at the flowering stage (Feekes 10.5) through to the milk-ripening stage (Feekes 11.1) [50], soil background still had an effect on the canopy spectral reflectance. The red-edge VIs, i.e., NREDI1, NREDI2, and NREDI3, were modifications of NDVI with red-edge1, red-edge2, and red-edge3, respectively, and the R^2 of models developed from these indices were 0.46, 0.42, and 0.21 respectively. The poor performances of these indices indicated that only using red-edge bands of sentinel-2 is insufficient for FHB monitoring. REHBI was developed from NIR-R and RE3-R, which have been proven to be sensitive to FHB severity. REHBI was defined as the area covered by a triangle in spectral reflectance space based on the reflectance of red, red-edge 3, and NIR regions. Therefore, information in the VIS, red-edge, and NIR regions were used. It achieved high monitoring accuracy, and the good performance of REHBI demonstrated the possibility of establishing disease monitoring indices based on basic VIs that are sensitive to disease severity. Figure 5 shows the performance of REHBI, OSAVI, and RDVI in identifying slightly and seriously diseased canopies. In general, REHBI performed better in monitoring slightly diseased canopies than other indices. As OSAVI and RDVI do not contain red-edge bands in their formulae, it is possible that red-edge bands provide important information for identifying slightly diseased canopies.

Poisson noise was added to the simulated multispectral data, and the performances of models developed from REHBI and fourteen commonly used VIs are shown in Table 3. As seen in the results of simulated multispectral data without Poisson noise, REHBI had slight variation in R^2 and RMSE values when noisy data was used, indicating that it has good resistance to Poisson noise. RDVI still performed best among conventional VIs ($R^2 = 0.69$, RMSE $= 13.4$). Regarding the red-edge VIs, the R^2 values of NREDI1, NREDI2, and NREDI3 were 0.26, 0.28, and 0.1, respectively, indicating that the combination of red-edge1 and red-edge3 could provide more information in monitoring the severity of diseased canopies. REHBI still performed best among all VIs ($R^2 = 0.74$, RMSE $= 12.6$). Thus, REHBI demonstrates high accuracy in monitoring the severity of diseased canopies, even when multispectral data contains Poisson noise.

In addition to the analysis of simulated Sentinel-2 data, FHB infection in wheat growing areas was monitored by applying REHBI, OSAVI, and RDVI to real Sentinel-2 imagery. The model developed based on REHBI was used to obtain the spatial distribution of FHB-infected and healthy winter wheat, as shown in Figure 6. In general, the wheat crop field of the study area was isolated, and the northwest part had more infected areas and a higher intensity of FHB infection compared to other regions, consistent with our field observations. The classification accuracy of the mapping results verified by direct field observation is shown in the confusion matrix in Table 4. The omission error and commission error of each class can be reflected by the producer's accuracy and the user's accuracy of diseased and healthy classes [51]. For the healthy class, REHBI produced a high producer's accuracy of 84%, while the user's accuracy also was 84%, indicating that REHBI was able to accurately identify healthy samples. OSAVI and RDVI both had a lower producer's accuracy of 74% and higher user's accuracy of 89%, indicating that they tended to misclassify diseased samples as healthy samples. For the diseased class, REHBI had higher user's accuracy and producer's accuracy than OSAVI and RDVI. Notably, the producer's accuracy of REHBI was 67%, while producer's accuracy of both OSAVI and RDVI was 33%, indicating that OSAVI and RDVI could not be used to accurately identify diseased samples. Consequently, REHBI demonstrated its superior ability to identify FHB at a regional scale.

There are still some challenges and limitations in monitoring FHB with REHBI at a regional scale. First, the hyperspectral data and field samples were acquired at the milk-ripening stage (Feekes 11.1). Therefore, it is unclear whether REHBI will perform well at other stages during FHB infection. Second, for the hyperspectral wheat canopy data used in the present study, the crop cultivars, cultivation procedures, and management practices of wheat field were uniform. In practice, these factors generally differ among the areas cultivated by individual smallholder farmers, so the diversity of these factors among cultivated areas should be considered to establish a more robust disease index for FHB monitoring. Third, although the monitoring method for simulated data and satellite borne data is different, it will be very interesting and meaningful to compare the accuracies of simulated data in relation to those of satellite borne data. Feature studies could analysis the difference of simulated data and satellite borne data, and compare the performance of these two kind of data. In addition, given the features they can sometimes share with FHB, confusion and uncertainties in disease monitoring can be caused by soil type, phenological different and some other environmental variables. In future research, the above factors should receive more attention in order to develop an even more robust and reliable FHB monitoring method at a regional scale.

V. CONCLUSION

Monitoring wheat FHB at a regional level plays an important role in agricultural management. This study proposed a new disease index, REHBI, to be used for monitoring wheat FHB. In the laboratory study, the simulated Sentinel-2 multispectral data were acquired from field canopy hyperspectral data. The basic VIs that were sensitive to the severity of disease were extracted from the dataset, and a disease index, i.e., REHBI, which was defined as the area covered by a triangle in spectral reflectance space based on the red, red-edge 3, and NIR reflectance values, was developed. The performance of REHBI was compared to those of some conventional VIs and red-edge VIs. All VIs showed different traits when monitoring the severity of wheat FHB, but REHBI performed the best among all VIs. The result showed that the REHBI tool proposed in this study can generate a reasonable wheat FHB damage map, and the overall accuracy is up to 78.6%. Thus, the REHBI could be used to monitor wheat FHB at a regional scale. Future studies should determine the breadth of situations in which this approach can be used, by, for example, evaluating the performance of REHBI when field samples are acquired at different times in the growing season. Further, consideration of more variables (e.g., soil type, cultivars) may improve the robustness and reliability of inferences made using this disease index.

REFERENCES

[1] Z. Cao, X. Yao, H. Liu, B. Liu, T. Cheng, Y. Tian, W. Cao, and Y. Zhu, "Comparison of the abilities of vegetation indices and photosynthetic parameters to detect heat stress in wheat," *Agricult. Forest Meteorol.*, vol. 265, pp. 121–136, Feb. 2019, doi: 10.1016/j.agrformet.2018.11.009.

[2] J. G. A. Barbedo, C. S. Tibola, and J. M. C. Fernandes, "Detecting Fusarium head blight in wheat Kernels using hyperspectral imaging," *Biosyst. Eng.*, vol. 131, pp. 65–76, Mar. 2015, doi: 10.1016/j.biosystemseng.2015.01.003.

[3] R. L. Whetton, K. L. Hassall, T. W. Waine, and A. M. Mouazen, "Hyperspectral measurements of yellow rust and Fusarium head blight in cereal crops: Part 1: Laboratory study," *Biosyst. Eng.*, vol. 166, pp. 101–115, Feb. 2018, doi: 10.1016/j.biosystemseng.2017.11.008.

[4] E. Bauriegel and W. Herppich, "Hyperspectral and chlorophyll fluorescence imaging for early detection of plant diseases, with special reference to Fusarium spec. Infections on wheat," *Agriculture*, vol. 4, no. 1, pp. 32–57, Mar. 2014, doi: 10.3390/agriculture4010032.

[5] L. Liu, Y. Dong, W. Huang, X. Du, J. Luo, Y. Shi, and H. Ma, "Enhanced regional monitoring of wheat powdery mildew based on an instance-based transfer learning method," *Remote Sens.*, vol. 11, no. 3, p. 298, Feb. 2019, doi: 10.3390/rs11030298.

[6] O. Mutanga, T. Dube, and O. Galal, "Remote sensing of crop health for food security in Africa: Potentials and constraints," *Remote Sens. Applications: Soc. Environ.*, vol. 8, pp. 231–239, Nov. 2017, doi: 10.1016/j.rsase.2017.10.004.

[7] Y. Shi, W. Huang, H. Ye, C. Ruan, N. Xing, Y. Geng, Y. Dong, and D. Peng, "Partial least square discriminant analysis based on normalized two-stage vegetation indices for mapping damage from rice diseases using PlanetScope datasets," *Sensors*, vol. 18, no. 6, p. 1901, Jun. 2018, doi: 10.3390/s18061901.

[8] J. Zhang, R. Pu, L. Yuan, J. Wang, W. Huang, and G. Yang, "Monitoring powdery mildew of winter wheat by using moderate resolution multi-temporal satellite imagery," *PLoS ONE*, vol. 9, no. 4, Apr. 2014, Art. no. e93107, doi: 10.1371/journal.pone.0093107.

[9] H. Ma, W. Huang, Y. Jing, C. Yang, L. Han, Y. Dong, H. Ye, Y. Shi, Q. Zheng, L. Liu, and C. Ruan, "Integrating growth and environmental parameters to discriminate powdery mildew and aphid of winter wheat using bi-temporal Landsat-8 imagery," *Remote Sens.*, vol. 11, no. 7, p. 846, Apr. 2019, doi: 10.3390/rs11070846.

[10] L. Yuan, J. Zhang, Y. Shi, C. Nie, L. Wei, and J. Wang, "Damage mapping of powdery mildew in winter wheat with high-resolution satellite image," *Remote Sens.*, vol. 6, no. 5, pp. 3611–3623, Apr. 2014, doi: 10.3390/rs6053611.

[11] P. D. Tapp and C. T. Siwak, "The use of high spectral resolution bands for estimating absorbed photosynthetically active radiation (A par)," in *Proc. Symp. Phys. Meas. Signatures Remote Sens.*, Val-d'Isère, France, 1994, pp. 415–434.

[12] T. Dong, J. Liu, J. Shang, B. Qian, B. Ma, J. M. Kovacs, D. Walters, X. Jiao, X. Geng, and Y. Shi, "Assessment of red-edge vegetation indices for crop leaf area index estimation," *Remote Sens. Environ.*, vol. 222, pp. 133–143, Mar. 2019, doi: 10.1016/j.rse.2018.12.032.

[13] W. Feng, B.-B. Guo, H.-Y. Zhang, L. He, Y.-S. Zhang, Y.-H. Wang, Y.-J. Zhu, and T.-C. Guo, "Remote estimation of above ground nitrogen uptake during vegetative growth in winter wheat using hyperspectral red-edge ratio data," *Field Crops Res.*, vol. 180, pp. 197–206, Aug. 2015, doi: 10.1016/j.fcr.2015.05.020.

[14] P. Griffiths, C. Nendel, and P. Hostert, "Intra-annual reflectance composites from Sentinel-2 and landsat for national-scale crop and land cover mapping," *Remote Sens. Environ.*, vol. 220, pp. 135–151, Jan. 2019, doi: 10.1016/j.rse.2018.10.031.

[15] T. Zheng, N. Liu, L. Wu, M. Li, H. Sun, Q. Zhang, and J. Wu, "Estimation of chlorophyll content in potato leaves based on spectral red edge position," *IFAC-PapersOnLine*, vol. 51, no. 17, pp. 602–606, 2018.

[16] Q. Zheng, W. Huang, X. Cui, Y. Shi, and L. Liu, "New spectral index for detecting wheat yellow rust using Sentinel-2 multispectral imagery," *Sensors*, vol. 18, no. 3, p. 868, Mar. 2018, doi: 10.3390/s18030868.

[17] W. J. Frampton, J. Dash, G. Watmough, and E. J. Milton, "Evaluating the capabilities of Sentinel-2 for quantitative estimation of biophysical variables in vegetation," *ISPRS J. Photogram. Remote Sens.*, vol. 82, pp. 83–92, Aug. 2013, doi: 10.1016/j.isprsjprs.2013.04.007.

[18] I. Dhau, E. Adam, O. Mutanga, K. Ayisi, E. M. Abdel-Rahman, J. Odindi, and M. Masocha, "Testing the capability of spectral resolution of the new multispectral sensors on detecting the severity of grey leaf spot disease in maize crop," *Geocarto Int.*, vol. 33, no. 11, pp. 1223–1236, Nov. 2018, doi: 10.1080/10106049.2017.1343391.

[19] M. Liu, T. Wang, A. K. Skidmore, and X. Liu, "Heavy metal-induced stress in rice crops detected using multi-temporal Sentinel-2 satellite images," *Sci. Total Environ.*, vols. 637–638, pp. 18–29, Oct. 2018, doi: 10.1016/j.scitotenv.2018.04.415.

[20] J. Xue and B. Su, "Significant remote sensing vegetation indices: A review of developments and applications," *J. Sensors*, vol. 2017, pp. 1–17, May 2017, doi: 10.1155/2017/1353691.

[21] A.-K. Mahlein, U. Steiner, H.-W. Dehne, and E.-C. Oerke, "Spectral signatures of sugar beet leaves for the detection and differentiation of diseases," *Precis. Agricult.*, vol. 11, no. 4, pp. 413–431, Aug. 2010.

[22] J. Hou, L. Li, and J. He, "Detection of grapevine leafroll disease based on 11-index imagery and ant colony clustering algorithm," *Precis. Agricult.*, vol. 17, no. 4, pp. 488–505, Aug. 2016.

[23] S. Bajwa, J. Rupe, and J. Mason, "Soybean disease monitoring with leaf reflectance," *Remote Sens.*, vol. 9, no. 2, p. 127, Feb. 2017, doi: 10.3390/rs9020127.

[24] H. AL-Saddik, J.-C. Simon, and F. Cointault, "Development of spectral disease indices for 'Flavescence Dorée' grapevine disease identification," *Sensors*, vol. 17, no. 12, p. 2772, Nov. 2017, doi: 10.3390/s17122772.

[25] C. Shan, W. Wang, C. Liu, Y. Sun, Q. Hu, X. Xu, Y. Tian, H. Zhang, I. Morino, D. W. T. Griffith, and V. A. Velazco, "Regional CO emission estimated from ground-based remote sensing at Hefei site, China," *Atmos. Res.*, vol. 222, pp. 25–35, Jul. 2019.

[26] W. Zhao and Y. Zou, "Hefei: An emerging city in inland China," *Cities*, vol. 77, pp. 158–169, Jul. 2018.

[27] X. Tao, J. Cui, Y. Dai, Z. Wang, and X. Xu, "Soil respiration responses to soil physiochemical properties in urban different green-lands: A case study in Hefei, China," *Int. Soil Water Conservation Res.*, vol. 4, no. 3, pp. 224–229, Sep. 2016.

[28] X. Liu, H. Liu, Y. Huang, and Y. Ye, "Relationships between nitrogen application rate soil nitrate-nitrogen, plant nitrogen concentration and wheat scab," *J. Plant Nutrition Fertilizer*, vol. 21, no. 2, pp. 306–317, 2015.

[29] L. Korhonen, H. Hadi, P. Packalen, and M. Rautiainen, "Comparison of Sentinel-2 and Landsat 8 in the estimation of boreal forest canopy cover and leaf area index," *Remote Sens. Environ.*, vol. 195, pp. 259–274, Jun. 2017.

[30] C. F. Jordan, "Derivation of leaf-area index from quality of light on the forest floor," *Ecology*, vol. 50, no. 4, pp. 663–666, Jul. 1969.

[31] A. J. Richardson and C. Wiegand, "Distinguishing vegetation from soil background information," *Photogramm. Eng. Remote Sens.*, vol. 43, no. 2, pp. 1541–1552, 1977.
[32] E. Bauriegel, A. Giebel, M. Geyer, U. Schmidt, and W. B. Herppich, "Early detection of *Fusarium* infection in wheat using hyper-spectral imaging," *Comput. Electron. Agricult.*, vol. 75, no. 2, pp. 304–312, 2011, doi: 10.1016/j.compag.2010.12.006.
[33] W. Huang, D. W. Lamb, Z. Niu, Y. Zhang, L. Liu, and J. Wang, "Identification of yellow rust in wheat using *in-situ* spectral reflectance measurements and airborne hyperspectral imaging," *Precis. Agricult.*, vol. 8, nos. 4–5, pp. 187–197, Nov. 2007.
[34] W. Huang, Q. Guan, J. Luo, J. Zhang, J. Zhao, D. Liang, L. Huang, and D. Zhang, "New optimized spectral indices for identifying and monitoring winter wheat diseases," *IEEE J. Sel. Topics Appl. Earth Observ. Remote Sens.*, vol. 7, no. 6, pp. 2516–2524, Jun. 2014.
[35] J. Zhang, R. Pu, W. Huang, L. Yuan, J. Luo, and J. Wang, "Using *in-situ* hyperspectral data for detecting and discriminating yellow rust disease from nutrient stresses," *Field Crops Res.*, vol. 134, pp. 165–174, Aug. 2012.
[36] R. Devadas, D. W. Lamb, S. Simpfendorfer, and D. Backhouse, "Evaluating ten spectral vegetation indices for identifying rust infection in individual wheat leaves," *Precis. Agricult.*, vol. 10, no. 6, pp. 459–470, Dec. 2009.
[37] J. W. Rouse, Jr., R. Haas, J. Schell, and D. Deering, "Monitoring vegetation systems in the great plains with ERTS," *NASA Special Publication*, vol. 351, p. 309, Jan. 1974.
[38] J. A. Gamon and J. S. Surfus, "Assessing leaf pigment content and activity with a reflectometer," *New Phytologist*, vol. 143, no. 1, pp. 105–117, Jul. 1999.
[39] A. A. Gitelson, Y. J. Kaufman, R. Stark, and D. Rundquist, "Novel algorithms for remote estimation of vegetation fraction," *Remote Sens. Environ.*, vol. 80, no. 1, pp. 76–87, Apr. 2002.
[40] F. Baret, S. Jacquemoud, and J. F. Hanocq, "The soil line concept in remote sensing," *Remote Sens. Rev.*, vol. 7, no. 1, pp. 65–82, Feb. 1993.
[41] J. M. Chen, "Evaluation of vegetation indices and a modified simple ratio for boreal applications," *Can. J. Remote Sens.*, vol. 22, no. 3, pp. 229–242, Sep. 1996.
[42] A. A. Gitelson, Y. J. Kaufman, and M. N. Merzlyak, "Use of a green channel in remote sensing of global vegetation from EOS-MODIS," *Remote Sens. Environ.*, vol. 58, no. 3, pp. 289–298, Dec. 1996.
[43] J.-L. Roujean and F.-M. Breon, "Estimating PAR absorbed by vegetation from bidirectional reflectance measurements," *Remote Sens. Environ.*, vol. 51, no. 3, pp. 375–384, Mar. 1995.
[44] A. Gitelson and M. N. Merzlyak, "Quantitative estimation of chlorophyll-*a* using reflectance spectra: Experiments with autumn chestnut and maple leaves," *J. Photochem. Photobiol. B, Biol.*, vol. 22, no. 3, pp. 247–252, Mar. 1994.
[45] A. Fernández-Manso, O. Fernández-Manso, and C. Quintano, "Sentinel-2A red-edge spectral indices suitability for discriminating burn severity," *Int. J. Appl. Earth Observ. Geoinf.*, vol. 50, pp. 170–175, Aug. 2016.
[46] R. Kutz and J. Sciulli, "The performance of an adaptive image data compression system in the presence of noise," *IEEE Trans. Inf. Theory*, vol. 14, no. 2, pp. 273–279, Mar. 1968.
[47] V. V. Lukin, M. S. Zriakhov, N. N. Ponomarenko, and A. Kaarna, "An automatic approach to lossy compression of images corrupted by Poisson noise," in *Proc. Microw., Radar Remote Sens. Symp.*, Sep. 2008, pp. 139–142.
[48] X. Jin, L. Jie, S. Wang, H. Qi, and S. Li, "Classifying wheat hyperspectral pixels of healthy heads and Fusarium head blight disease using a deep neural network in the wild field," *Remote Sens.*, vol. 10, no. 3, p. 395, Mar. 2018, doi: 10.3390/rs10030395.
[49] B. Jaillais, P. Roumet, L. Pinson-Gadais, and D. Bertrand, "Detection of Fusarium head blight contamination in wheat Kernels by multivariate imaging," *Food Control*, vol. 54, pp. 250–258, Aug. 2015, doi: 10.1016/j.foodcont.2015.01.048.
[50] J. S. West, G. G. M. Canning, S. A. Perryman, and K. King, "Novel technologies for the detection of Fusarium head blight disease and airborne inoculum," *Tropical Plant Pathol.*, vol. 42, no. 3, pp. 203–209, Jun. 2017, doi: 10.1007/s40858-017-0138-4.
[51] J. R. B. Fisher, E. A. Acosta, P. J. Dennedy-Frank, T. Kroeger, and T. M. Boucher, "Impact of satellite imagery spatial resolution on land use classification accuracy and modeled water quality," *Remote Sens. Ecol. Conservation*, vol. 4, no. 2, pp. 137–149, Jun. 2018.

LINYI LIU received the B.S. degree in geographic information system from Capital Normal University, Beijing, China, in 2015. He is currently pursuing the Ph.D. degree with the Aerospace Information Research Institute, Chinese Academy of Sciences, Beijing. His current research interests include crop disease monitoring, remote sensing, and geographic information systems.

YINGYING DONG received the B.S. degree in information and computation science from Shandong Normal University, Shandong, China, in 2006, the M.S. degree in mathematics of computation from Capital Normal University, Beijing, China, in 2009, and the Ph.D. degree in agricultural remote sensing and information technology from Zhejiang University, Zhejiang, China, in 2013. Her research interest includes research and application in vegetation remote sensing.

WENJIANG HUANG received the Ph.D. degree in cartography and GIS from Beijing Normal University, Beijing, China, in 2005. He is currently a Professor with the Key Laboratory of Digital Earth Science, Institute of Remote Sensing and Digital Earth, Chinese Academy of Sciences, Beijing. His research interests include quantitative remote sensing research and application in vegetation.

XIAOPING DU received the B.S. and M.S. degrees in computing science and technology from the China University of Geosciences, China, in 2001 and 2004, respectively, and the Ph.D. degree in GIS from the University of Chinese Academy of Sciences, in 2015. From 2016 to 2018, he held a postdoctoral position with the German Aerospace Center (DLR). He is currently an Associate Professor with the Institute of Remote Sensing and Digital Earth, Chinese Academy of Sciences. His research interests include digital earth, geospatial big data, remote sensing for natural disasters, and environment monitoring.

BINYUAN REN received the M.S. degree from Nanjing Agricultural University, Nanjing, China, in 2014. His current research interests include crop pests and disease monitoring and forecasting, and crop pests and disease control technique extension.

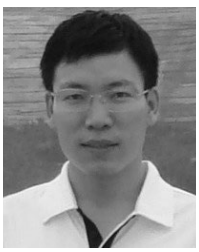

LINSHENG HUANG received the Ph.D. degree in circuits and systems from Anhui University, Hefei, China, in 2013. He is currently a Professor with the Key Laboratory of Intelligent Computing and Signal Processing, Ministry of Education, Anhui University. His research interests include remote sensing, image processing technology, and applications of vegetation.

QIONG ZHENG received the Ph.D. degree from the College of Geosciences and Surveying Engineering, China University and Mining and Technology, Beijing, China, in 2009, and the Ph.D. degree from the Key Laboratory of Digital Earth Science, Institute of Remote Sensing and Digital Earth, Chinese Academy of Sciences, Beijing. She is currently an Assistant Researcher with the Guangzhou Institute of Geography. Her current research interests include precision agricultural management, hyperspectral analyzing, and crop diseases detection and monitoring by remote sensing data.

HUIQIN MA received the B.S. and M.S. degrees in applied meteorology from the Nanjing University of Information Science and Technology, China, in 2014 and 2017, respectively, where she is currently pursuing the Ph.D. degree. Her current research interests include agro-meteorology and quantitative remote sensing of vegetation.